Comparative Study of Reaction Centers from Photosynthetic Purple Bacteria: Electron Paramagnetic Resonance and Electron Nuclear Double Resonance Spectroscopy†

J. Rautter, F. Lendzian, and W. Lubitz*

Max-Volmer-Institut für Biophysikalische und Physikalische Chemie, Technische Universität Berlin, Strasse des 17.Juni 135, D-10623 Berlin, Germany

S. Wang and J. P. Allen

Department of Chemistry and Biochemistry and the Center for the Study of Early Events in Photosynthesis, Arizona State University, Tempe, Arizona 85287-1604

Received March 14, 1994; Revised Manuscript Received July 25, 1994®

ABSTRACT: Reaction centers (RCs) from four species of purple bacteria, *Rhodobacter sphaeroides*, *Rhodobacter capsulatus*, *Rhodospirillum rubrum*, and the recently discovered bacterium *Rhodospirillum centenum*, have been characterized by optical spectroscopy [Wang, S., Lin, X., Woodbury, N. W., & Allen, J. P. (1994) *Photosynth. Res.* (submitted for publication)] and magnetic resonance spectroscopy. All RCs contain a bacteriochlorophyll (BChl) *a* dimer as the primary donor. For *Rb. sphaeroides* and *Rs. rubrum* the donor Q_Y optical band is at ~865 nm, compared to ~850 nm for *Rb. capsulatus* and *Rs. centenum*. The primary donor in the RCs can be converted between these two forms by the addition or removal of charged detergents. The electronic structure of the cation radical of the primary electron donor $P^{+\bullet}$ was investigated in these species using electron paramagnetic resonance (EPR), electron nuclear double resonance (ENDOR), and electron nuclear triple resonance (TRIPLE) spectroscopy. The EPR line widths of $P^{+\bullet}$ vary significantly and the ENDOR and Special TRIPLE spectra reveal drastic differences in the spin density distribution of the dimer for the different species. Reaction centers from *Rb. sphaeroides* and *Rs. rubrum* have a slightly asymmetric spin density distribution over the two halves of the dimer. The respective ratios are 2:1 and 1.6:1 in favor of the L-half of the BChl *a* dimer. In contrast, the spectra of $P^{+\bullet}$ in reaction centers from *Rb. capsulatus* and *Rs. centenum* show an almost complete localization of the unpaired electron on the L-half of the dimer (ratio ~5:1). The different spin density distributions in the four species are discussed in the framework of a simple theoretical model for the dimer [Plato, M., Lendzian, F., Lubitz, W., & Möbius, K. (1992) in *The Photosynthetic Bacterial Reaction Center II: Structure, Spectroscopy and Dynamics* (Breton, J., & Vermeglio, A., Eds.) pp 99–108, Plenum Press, New York]. In this model the observed asymmetries are attributed to different orbital energies of the two BChl *a* halves of the dimer. Possible reasons for the energetic inequivalencies of the dimer halves are discussed. The observed orbital asymmetries in the primary donor cation radicals correlate with the different Q_Y absorption bands of P and also with the different charge recombination rates from the primary quinone in these species. In contrast to the results obtained for reaction centers, the electron spin density distribution of $P^{+\bullet}$ is identical in chromatophores of all four investigated bacterial species and corresponds to a ratio of 2:1 in favor of the L half of the dimer. These results indicate that the environment of the reaction centers influences both the electronic structure of the cofactors and the electron transfer rates.

In bacterial photosynthesis the light-induced electron transfer reactions occur in a pigment–protein complex called the reaction center (RC).[1] Despite the arrangement of the pigment molecules in two branches (A- and B-branch), which are related by an approximate C_2 symmetry axis (Deisenhofer et al., 1984; Allen et al., 1987; El-Kabbani et al., 1991), the charge separation occurs only via the A-branch.

This charge separation process is determined by both the three-dimensional arrangement and the electronic structure of the interacting pigment molecules. To obtain the electronic structure of the radical cations and anions formed in the electron transfer process, "hyperfine spectroscopy", such as electron nuclear double resonance (ENDOR), can be utilized. After the measured hyperfine coupling constants (hfcs) are assigned to molecular positions, a map of the spin density distribution over the investigated molecule is obtained [for reviews see Möbius et al. (1989) and Lubitz (1991)].

Of particular importance is the investigation of the cofactor initiating the electron transfer in the RC, the primary electron donor P, which is a "special pair" of bacteriochlorophyll (BChl) molecules with an optical absorption band near ~865 nm. The two halves of this dimer are denoted P_L and P_M; L and M indicate the protein subunits to which the two BChls are bound. Figure 1 shows the structure of BChl *a*. Two Bchl

† This work was supported by DFG (Sfb 312, TP A4), NATO (CRG 910468), Fonds der Chemischen Industrie to W. L., and NIH (GM41300) to J.P.A. This is publication 208 from the Center for Early Events in Photosynthesis. The Center is funded by DOE Grant DE-FG-88-ER 13969 as a part of the USDA/DOE/NSF Plant Science Centers Program.

* Author to whom correspondence should be addressed.

® Abstract published in *Advance ACS Abstracts,* September 1, 1994.

[1] Abbreviations: RC, reaction center; P, primary donor; $P^{+\bullet}$, primary donor cation radical; Q, quinone; BChl, bacteriochlorophyll; LDAO, *N*,*N*-dimethyldodecylamine *N*-oxide; DOC, deoxycholate; Tris, tris(hydroxymethyl)aminomethane; EDTA, ethylenediaminetetraacetic acid; EPR, electron paramagnetic resonance; ENDOR, electron nuclear double resonance; hfc, hyperfine coupling constant; MO, molecular orbital; DOC, deoxycholate; rf, radio frequency.

0006-2960/94/0433-12077$04.50/0

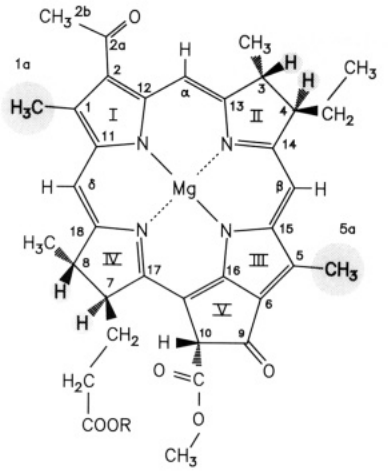

FIGURE 1: Molecular structure of BChl *a*, including numbering scheme. The isoprenoid chain, R., is either geranylgeranyl as in RCs on *Rs. rubrum* or phytyl as in *Rb. sphaeroides*. The proton positions exhibiting large hfcs in the cation radical are indicated by shaded circles.

a molecules constitute the primary donor in all investigated species.

Recent electron paramagnetic resonance (EPR) and ENDOR studies of the cation radical of the primary donor $P^{+\bullet}$ in single crystals of *Rhodobacter sphaeroides* R-26 revealed an unequal spin density distribution of the unpaired electron with a ratio of 2:1 in favor of the L-half of the dimer, P_L (Lendzian et al., 1993). A similar ratio was also found for $P^{+\bullet}$ in *Rhodopseudomonas viridis* (Lendzian et al., 1988). The observed asymmetry was attributed to energetic differences of the highest filled molecular orbitals of the monomeric halves P_L and P_M in the framework of a simple Hückel molecular orbital (HMO) model dimer (Plato et al., 1992; Lendzian et al., 1993). A similar but more elaborate dimer model was introduced to explain the new absorption bands attributed to $P^{+\bullet}$ at 2600 cm^{-1} in *Rb. sphaeroides* and 2750 cm^{-1} in *Rps. viridis* (Breton et al., 1992; Parson et al., 1992). These results prompt the question whether the asymmetric spin density distribution in favor of the L-half of the primary donor is a common feature which is shared also by other purple bacteria and if the function of the RC is related to this asymmetry. Here, we present an EPR/ENDOR investigation of the spin density distribution of the primary donor cation radical $P^{+\bullet}$ in RCs and chromatophores of four species of purple bacteria, all containing Bchl *a*. The obtained orbital asymmetries of the donors from the four species are then related to the electron transfer and recombination rates that have been published elsewhere (Wang et al., 1994).

MATERIALS AND METHODS

The growth conditions and isolation protocols of the RCs from *Rb. sphaeroides* R-26, *Rhodobacter capsulatus*, and *Rhodospirillum centenum* have been described in Wang et al. (1994). Briefly, the RCs were solubilized from chromatophores with the detergent *N*,*N*-dimethyldodecylamine *N*-oxide (LDAO) and purified by use of a DEAE-Sephacel column with the RCs eluting at a salt concentration of ~120 mM. The most pure fractions were collected, concentrated, and dialyzed against 10 mM potassium phosphate, pH 7.4, and 0.05% LDAO (*Rb. capsulatus*) or 200 mM NaCl, 15 mM Tris-HCl, pH 8, 0.025% LDAO, and 1 mM EDTA (*Rs. centenum*). *Rhodospirillum rubrum* G-9 was grown anaerobically in the light in a modified Hutners medium. RCs were isolated with 0.565% LDAO and purified by a sucrose gradient (5–25%) followed by gel filtration (Sepharose Cl-6B and Bio-Gel A50m). After purification, RCs were stored at pH 7.5 with 15 mM Tris-HCl, 1 mM EDTA, and 0.02% LDAO.

For the EPR/ENDOR and Special TRIPLE measurements, RCs of *Rb. capsulatus* in 10 mM potassium phosphate buffer, pH 7.4, and 0.1% LDAO, were concentrated to $A_{802}^{1cm} \approx 80$. RCs of *Rs. centenum* in 60 mM NaCl, 15 mM Tris-HCl, pH 8, 0.1% LDAO, and 1 mM EDTA were concentrated to $A_{802}^{1cm} \approx 30$. *Rs. rubrum* wild-type RCs in 15 mM Tris-HCl, pH 8.0, 1 mM EDTA, and 0.025% LDAO with 60 mM NaCl were concentrated to $A_{802}^{1cm} \approx 100$. RCs of *Rs. rubrum* G-9 were in 15 mM Tris-HCl, 1 mM EDTA, and 0.02% LDAO at pH 7.5 and were concentrated to $A_{802}^{1cm} \approx 70$. Chromatophores from all four species were concentrated to $A_{865}^{1cm} \approx 200$.

EPR/ENDOR Spectroscopy. The EPR and ENDOR measurements were performed on a Bruker ESP 300E spectrometer with home-built ENDOR and TRIPLE resonance accessories. The control of the ENDOR instrumentation is performed using the computer subsystem of the ESP 300E EPR instrument by a locally written program. This program, which is used for experimental control and acquisition of data, is interfaced to the main ESP program. For EPR a standard rectangular cavity (Bruker ER 4102 ST) was used, whereas the ENDOR and Special TRIPLE investigations were carried out using a TM_{110} cavity of local design with a specially designed radio frequency (rf) coil providing a high quality factor Q (unloaded) = 5000 (Thanner, 1990). This cavity is very similar to the one described in Zweygart et al. (1994), but the resonance structure is made from brass instead of quartz and the microwave coupling is through a semirigid coaxial cable instead of a waveguide.

The experiments on RCs in liquid solution were performed in Pyrex capillaries of 1-mm inner diameter to minimize dielectric losses. The cation radical of the primary donor, $P^{+\bullet}$, was generated by continuous illumination of the sample inside the cavity with a 100-W tungsten halogen lamp filtered to allow transmission of light in the range of 830–900 nm. Nitrogen gas cooling using a Bruker ER 4111 VT temperature control system was employed. The RC and chromatophore samples for the frozen solution measurements were prepared in quartz tubes (i.d. 3 mm). For RCs 65% (v/v) glycerol was used as cryoprotectant. While being stirred, the samples were illuminated for 10–20 s at room temperature using the light conditions described above prior to freezing in liquid nitrogen.

RESULTS

The EPR spectra of $P^{+\bullet}$ in RCs of all four investigated species consist of Gaussian envelopes and show no resolved hyperfine structure (see Figure 2). The measured line widths ΔB_{pp} are different in the four species and increase from 0.92 mT for *Rs. rubrum* to 0.95 mT for *Rb. sphaeroides*, 1.10 mT for *Rb. capsulatus*, and 1.12 mT for *Rs. centenum* (Table 1). For a symmetric distribution of the unpaired electron over the two dimer halves, a $2^{-1/2}$ narrowing of the EPR line width with respect to the line width of the monomeric BChl $a^{+\bullet}$ (ΔB_{pp} = 1.40 mT) is expected. The observed line narrowing of $P^{+\bullet}$ in *Rb. sphaeroides* led to the proposal that P is a BChl *a* dimer (Norris et al., 1971). For asymmetric spin density distributions, line widths with values between the monomer and the symmetric dimer case are expected (Lendzian et al., 1993). Therefore, the line width variations observed for the different bacterial RCs (Figure 2) provide a first hint for

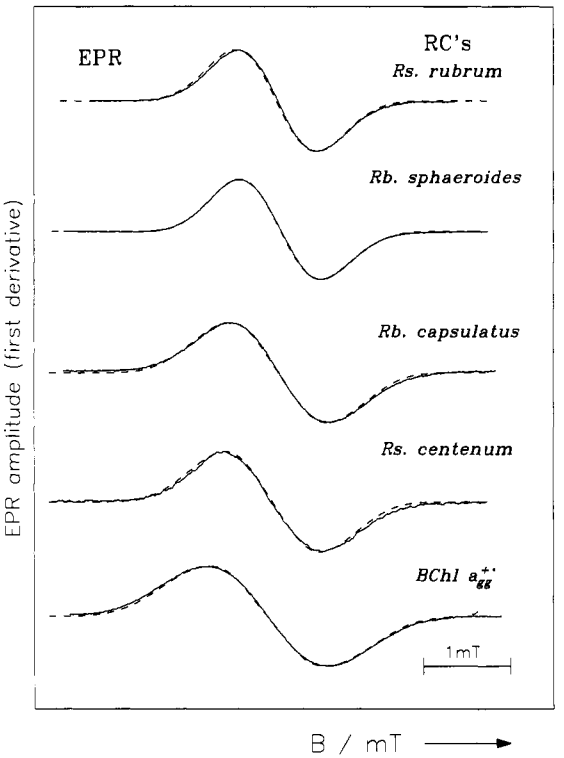

FIGURE 2: Experimental (solid lines) and simulated (dashed lines) EPR spectra of photoinduced $P^{+}\cdot$ in liquid solutions of RCs of the four investigated purple bacteria and of BChl $a^{+}\cdot$. The Gaussian envelope peak-to-peak line widths ΔB_{pp} are collected in Table 1. Experimental conditions: $T \approx 293$ K, microwave power ≈ 1 mW, field modulation 100 kHz, depth: 0.1–0.2 mT, scan time 15 min. For the simulations the hfcs and assignments given in Table 1 were used. Remaining ^{1}H hfcs, not resolved in the ENDOR and special TRIPLE spectra, and the ^{14}N hfcs were estimated for P_L and P_M by scaling the respective values of BChl $a^{+}\cdot$ (Lubitz, 1991) with the appropriate spin density ratios given in Table 1.

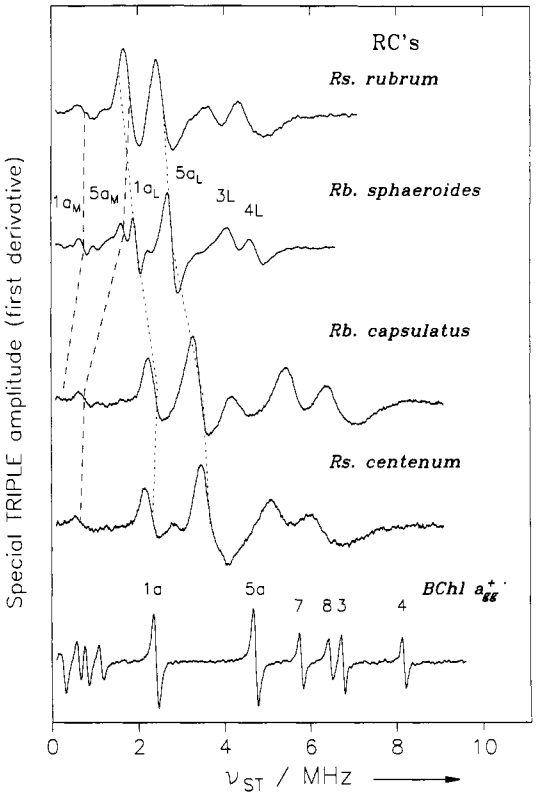

FIGURE 3: Comparison of the ^{1}H Special TRIPLE spectra of $P^{+}\cdot$ in RCs of the investigated purple bacteria with BChl $a_{gg}^{+\cdot}$ (iodine oxidation, CH_2Cl_2:CH_3OH = 6:1). In this type of electron–nuclear–nuclear TRIPLE resonance experiment both high- and low-frequency ENDOR transitions, which are symmetrically displaced around the proton Larmor frequency, $\nu_{ENDOR}^{\pm} = |\nu_H \pm {}^{1}/_{2}A_{iso}|$, are induced simultaneously. Special TRIPLE line intensities are larger than those in ENDOR spectroscopy and less dependent on temperature. The frequency scale gives the deviation from the Larmor frequency; thus, each line position corresponds to half the respective hfc. For *Rb. sphaeroides* R-26 and for BChl $a_{gg}^{+\cdot}$ the assignments of spectral lines (hfcs) to molecular positions is given (for numbering see Figure 1). The change of line positions for $P^{+}\cdot$ in the other RCs with respect to *Rb. sphaeroides* is indicated by dashed ($1a_M$, $5a_M$) and dotted ($1a_L$, $5a_L$) lines; see text. Experimental conditions: (i) *Rs. rubrum*, *Rb. capsulatus*, and *Rs. centenum*, T = 15 °C, rf power 2 × 150 W, microwave power 20 mW, rf modulation depth 200 kHz (frequency 12.5 kHz), accumulation time 2 h; (ii) for *Rb. sphaeroides* and BChl $a^{+}\cdot$, see Lendzian et al. (1993) and Lubitz et al. (1984), respectively.

different degrees of delocalization of the unpaired electron in the dimer.

In Figure 3 the Special TRIPLE spectra of $P^{+}\cdot$ in RCs of *Rs. rubrum*, *Rb. sphaeroides*, *Rb. capsulatus*, and *Rs. centenum* are compared with that of the BChl *a* cation radical *in vitro*. The spectra obtained for $P^{+}\cdot$ are quite well resolved. A spectral deconvolution program (Tränkle & Lendzian, 1989) was used for a more detailed analysis of overlapping lines in the spectra (data not shown). Up to eight hfcs were obtained for $P^{+}\cdot$, which are all collected in Table 1.

For $P^{+}\cdot$ in RCs of *Rb. sphaeroides*, the hfcs have recently been unambiguously assigned to molecular positions in the dimer by ENDOR experiments that were performed on RC single crystals (Lendzian et al., 1993). The most prominent hfcs arise from the β-protons of rings II and IV and the methyl protons at positions 1a and 5a (see Figures 1 and 3). Analysis of the spectra from the RC single crystals yielded an asymmetric spin density distribution of approximately 2:1 in favor of the L-half of the BChl *a* dimer (see Table 1).

In the Special TRIPLE spectra of $P^{+}\cdot$ (Figure 3) the intensities of the lines decrease considerably toward smaller frequencies. The intensity change is due to a nonselective EPR saturation of the individual hyperfine lines belonging to small hfcs (Allendoerfer & Maki, 1970) that is caused by the large homogeneous EPR line width of the slowly tumbling RC complex in solution. The effect is best seen for the well-resolved four methyl lines in the spectrum of $P^{+}\cdot$ in *Rb. sphaeroides* (Figure 3). In the Special TRIPLE spectrum of $P^{+}\cdot$ in *Rs. rubrum*, spectral deconvolution shows that the two lines belonging to the methyl groups $5a_M$ and $1a_L$ coincide and thus lead to a large intensity of the line at 1.8 MHz (Figure 3).

Identification of the hfcs of the methyl protons of $P^{+}\cdot$ in *Rb. capsulatus*, *Rs. centenum*, and *Rs. rubrum* RCs was achieved by a comparison of liquid and frozen solution spectra. This is based upon the observation that only protons of freely rotating methyl groups give rise to sharp and intense ENDOR lines in frozen solutions (Hyde et al., 1968; Feher et al., 1975). In Figure 4 the liquid solution ENDOR spectrum of *Rb. capsulatus* (Figure 4a) is compared with the frozen solution spectra of *Rb. capsulatus* (Figure 4b) and *Rs. centenum* (Figure 4c). In the frozen state the lines of the smallest methyl coupling ($1a_M$) are also clearly visible whereas in the liquid solution they are suppressed (see above). In this way the four methyl group hfcs (positions 5a and 1a in P_L and P_M) could be identified in all four species; the corresponding hfcs are presented in Table 1.

As noted by Feher (1992), the methyl proton hfcs at positions 1a and 5a (see Figure 1) exhibit characteristic ratios for the L and M halves (P_L and P_M) of the dimer in *Rb. sphaeroides*.

Table 1: ^{1}H hfcs,[a] Ratios of hfcs, and EPR Line Widths for $P^+\bullet$ in the Investigated Bacterial RCs and for BChl $a^+\bullet$

	$P^+\bullet$				
	Rb. sphaeroides[b]	*Rs. rubrum*[c]	*Rb. capsulatus*	*Rs. centenum*	BChl $a_{gg}^{+\bullet}$[d]
$A(5a_L)$[e]	5.61	5.15	7.00	7.20	
$A(1a_L)$	3.95	3.55	4.90	4.60	9.50 (5a)
$A(5a_M)$	3.41	3.90	1.55	1.50	4.85 (1a)
$A(1a_M)$	1.48	1.60	0.65[f]	0.60[f]	
$\sum A(CH_3)$[g]	14.45	14.20	14.10	13.90	14.35
$A(\beta_L)$[h]	9.50 (4)	9.10	13.20	12.55	16.43 (4)
	8.46 (3)	7.50	11.50	10.75	13.59 (3)
			8.50	8.50	13.00 (7)
				5.80	11.61 (8)
$[A(5a)/A(1a)]_L$[i]	1.42	1.45	1.43	1.56	
					1.96
$[A(5a)/A(1a)]_M$[i]	2.30	2.43	2.38	2.50	
$\sum A(CH_3)_L/[\sum A(CH_3)_L + \sum A(CH_3)_M]$[j]	0.66	0.61	0.84	0.85	1.0
ΔB_{pp} [mT] exp[k]	0.95	0.92	1.10	1.12	1.40
ΔB_{pp} [mT] sim[k]	0.95	0.92	1.10	1.12	1.40

[a] All hfcs are given in megahertz and are from liquid solution spectra (Figure 3) unless otherwise stated; errors of CH_3 hfcs ±30 kHz and of β hfcs ±50 kHz. [b] Proton hfcs taken from Lendzian et al. (1993). [c] The assignments given in this paper differ from our earlier work (Lubitz et al., 1984), where only two hfcs were assigned to methyl protons and were interpreted in terms of a symmetric dimer. [d] Proton hfcs taken from Lubitz et al. (1984); side chain geranylgeranyl. The values in parentheses give the assignments to molecular positions (see Figure 1); the same values hold for BChl a_p from *Rb. sphaeroides* (side chain phytyl). [e] For numbering of positions (in parentheses) see Figure 1; for assignments see text. [f] These hfcs were obtained from frozen solution spectra (Figure 4), error ±70 kHz. [g] Sum of all four methyl proton hfcs. [h] β-proton hfcs (positions 4, 3, 7, and 8 in Figure 1), only the largest clearly resolved hfcs assigned to P_L are given. In the range of the smaller couplings several additional lines were resolved, which were tentatively assigned to β protons of rings II and IV of P_M. [i] Ratio of methyl proton hfcs at positions 5a and 1a on P_L and P_M, respectively (see text). [j] Fraction of spin density on P_L as measured from the CH_3 hfcs at positions 1a and 5a. [k] Experimental and simulated peak-to-peak Gaussian envelope EPR line width; see Figure 2.

This is due to different geometries of the BChl *a* molecules constituting the dimer. The effect could be caused by different rotation angles of the acetyl groups in the two dimer halves (Plato et al., 1986, 1992). The ratios are $A(5a)/A(1a) = 1.42$ for P_L and $A(5a)/A(1a) = 2.30$ for P_M (see Table 1). These ratios of hfcs were found to be conserved in several mutants of *Rb. sphaeroides* in spite of significant shifts of spin density between P_L and P_M (Rautter et al., 1992). Our assignments of the methyl protons of P_L and P_M given in Table 1 are based on the assumption that these ratios are also conserved in the other three species investigated in this paper.

With this assumption, the large methyl hfcs of 7.0 and 4.9 MHz of $P^+\bullet$ in RCs of *Rb. capsulatus* were assigned to positions 5a and 1a in P_L, respectively, whereas the small methyl couplings of 1.55 and 0.65 MHz were assigned to the 5a and 1a positions, respectively, in P_M (see Table 1). Since the magnitudes of β-proton hfcs are strongly dependent on the exact geometries of the hydrogenated rings II and IV (Forman et al., 1989; Käss et al., 1994), only the methyl hfcs were used for an evaluation of the spin density distribution of $P^+\bullet$. This approach leads to an asymmetric spin density distribution with 84% of the spin density on P_L. A similar extent of localization of the unpaired electron on the L-half of the dimer is found for *Rs. centenum*. The observed large methyl coupling constants of 7.2 and 4.6 MHz lead to a spin density distribution with 85% on P_L. From the spectrum of *Rs. rubrum* wild type (see Figure 3) we obtain a spin density of 61% on P_L, which is close to the value found for *Rb. sphaeroides* (66%).

The fairly constant ratios of the hfcs of position 5a to 1a in P_L and P_M obtained in all four species (see Table 1) support our assignment of the larger spin densities to P_L. The sum of all methyl hfcs in $P^+\bullet$ and also in the BChl *a* cation radical remains remarkably constant (Table 1). This shows that there is no redistribution of spin densities within each BChl *a* moiety, P_L and P_M, as compared with *Rb. sphaeroides*. The main difference between the RCs of the investigated species is a shift of spin density between P_L and P_M.

Our result, that the spin density distribution in the different species is asymmetric in favor of P_L, is in agreement with recent near-infrared resonance Raman Fourier transform investigations, in which a predominant charge localization on P_L was observed for $P^+\bullet$ in RCs of *Rb. sphaeroides*, *Rs. rubrum*, and *Rb. capsulatus* (Mattioli et al., 1992).

The large β-proton hfcs given in Tables 1 and 2 were also assigned to P_L in analogy to the large methyl hfcs. The observed EPR line widths can be simulated using the respective hfcs and spin density ratios (Tables 1 and 2). The EPR simulations are shown together with the experimental spectra in Figure 2.

The hfcs measured for $P^+\bullet$ in RCs of *Rs. rubrum* wild type differ slightly from the respective values obtained for the carotenoidless mutant *Rs. rubrum* G-9 (Lubitz et al., 1984). Since the RC preparation reported in Lubitz et al. (1984) contained Triton as detergent instead of LDAO as used in this paper, we performed additional Special TRIPLE experiments on *Rs. rubrum* G-9 with LDAO as detergent. The obtained hfcs showed that the spin densities of $P^+\bullet$ in RC's of *Rs. rubrum* G-9 are identical within the experimental error in the two different detergents (Table 2). Therefore it is concluded that these detergents have no significant influence on the spin density distribution. However, the data indicate a shift of spin density toward P_L (+2%) in the wild type as compared with the mutant G-9. Although this effect is very small and close to the experimental resolution limits, the opposite directions of the shifts for the lines assigned to the L and M half in *Rs. rubrum* wild type can be clearly obtained from the spectra. A similar effect has been observed for $P^+\bullet$ in *Rb. sphaeroides* wild type and the carotenoidless mutant R-26 in single-crystal ENDOR experiments (Gessner et al., 1992). This effect is attributed to the lack of the carotenoid in the mutant RCs, which is located near the accessory BChl of the B-branch in the wild type (Yeates et al., 1988). This BChl is quite close to the dimer and a change in its binding could cause a slight structural distortion of the binding site of the primary donor. However, the effect of the lack of the carotenoid molecule on the spin density distribution of $P^+\bullet$ is much smaller than the differences found for the two classes of the investigated RCs. Therefore, the different carotenoid molecules present in the four species, i.e., spirilloxanthin in

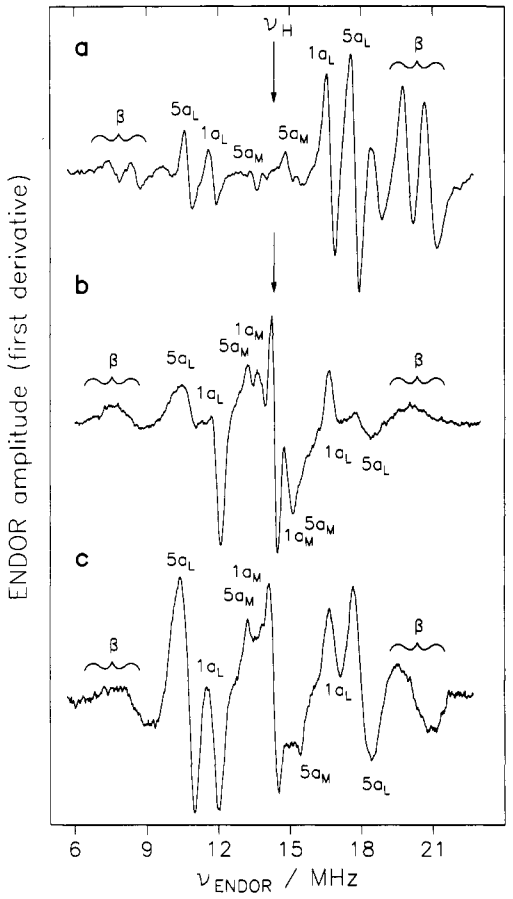

FIGURE 4: ENDOR spectra of P^+ • in RCs of *Rb. capsulatus* in liquid (a) and frozen (b) solutions of RCs and P^+ • in frozen solution of RCs from *Rs. centenum* (c). In the frozen solution spectra only the lines of the methyl protons (positions $1a_M$, $5a_M$, $1a_L$, and $5a_L$) remain narrow and intense due to the small hyperfine anisotropy and the fast rotation of the methyl groups even at low temperatures (see text). The outermost lines belonging to the β-protons of the saturated rings II and IV (see Figure 1) are considerably broadened under these conditions. In spectrum (b) the line pair belonging to the methyl group with the smallest hfc (position $1a_M$) is clearly resolved. In spectrum (c) it is seen as shoulders on the proton matrix line near 14 MHz and can be obtained by spectral deconvolution. Experimental conditions: (a) T = 290 K, microwave power 16 mW, rf power 200 W, rf modulation depth 150 kHz (frequency 12.5 kHz), accumulation time 2 h; (b and c) T = 150 K, microwave power 4 mW, rf power 150 W, rf modulation depth 200 kHz (frequency 12.5 kHz), accumulation time 1 h.

Rs. rubrum and spheroidene in *Rb. sphaeroides* and *Rb. capsulatus*, cannot be responsible for the observed shifts of spin densities.

For reasons of stability of the RC preparations of *Rs. rubrum* wild type and *Rs. centenum*, 60 mM NaCl was present in the solution. In the case of *Rs. rubrum* wild type RC, spectra were also taken from samples in which the salt was removed by dialysis. These samples gave identical spectra for P^+ •. It is therefore concluded that the salt concentration used in our experiments had no effect on the electronic structure of P^+ •.

The position of the optical absorption band characteristic for P is different in the four RCs investigated (Table 3). In particular, for *Rb. capsulatus* and *Rs. centenum* the dimer band is blue-shifted by up to 15 nm. This was attributed by Wang et al. (1994) to the loss of charged phospholipids in the surrounding of the RC during the isolation process since the absorption band can be shifted back to 865 nm, where is is found in *Rb. sphaeroides*, by addition of charged detergents like deoxycholate (DOC).

Table 2: Comparison of ^1H hfcs A and Ratios of hfcs for P^+ • in RCs of *Rs. rubrum* and *Rb. capsulatus* with Different Detergents[a]

	Rs. rubrum			*Rb. capsulatus*	
	wild type, LDAO	G-9, LDAO	G-9, Triton	0.1% DOC[b]	without DOC
$A(5a_L)$[c]	5.15	4.80	4.80	5.35	7.00
$A(1a_L)$	3.55	3.40	3.35	3.50	4.90
$A(5a_M)$	3.90	4.00	3.95	3.95	1.55
$A(1a_M)$	1.60	1.65	1.65	1.90	0.65
$\Sigma A(CH_3)$[d]	14.20	13.85	13.75	14.70	14.10
$A(\beta_L)$[e]	9.10	9.00	8.80	8.70	13.20
	7.50	7.15	7.10	7.25	11.50
$[A(5a)/A(1a)]_L$[f]	1.45	1.41	1.43	1.52	1.43
$[A(5a)/A(1a)]_M$[f]	2.44	2.42	2.39	2.19	2.38
$\Sigma A(CH_3)_L/[\Sigma A(CH_3) + \Sigma A(CH_3)_M]$[g]	0.61	0.59	0.59	0.60	0.84

[a] All hfcs are given in megahertz. For all hfcs from ENDOR (Figures 3, 4, and 5), the estimated maximum errors obtained from liquid solutions are ±30 kHz for all methyl proton hfcs and ±50 kHz for all β-protons hfcs; the error of $A(1a_M)$ of *Rb. capsulatus* without DOC obtained in frozen solution is ±70 kHz. [b] Only the values of the distinct second species are given; see Figure 5c. [c] For numbering of positions (in parentheses) see Figure 1; for assignments see text. [d] Sum of all four methyl proton hfcs. [e] β-protons hfcs (positions 4, 3, 7, and 8 in figure 1); only the two largest, clearly resolved hfcs assigned to P_L are given for comparison (see Table 1). [f] Ratio of methyl proton hfcs at positions 5a and 1a on P_L and P_M, respectively (see text). [g] Fraction of spin density on the dimer half P_L as obtained from the CH_3 hfcs at positions 1a and 5a.

Table 3: Comparison of the Donor Q_y bands, Spin Density Ratios, and the $P^+Q_A^-$ to PQ_A Recombination Rates for the Investigated Bacterial RCs

species	donor Q_y band[a] (nm)	spin density ratios[b]	recombination rate (s^{-1})[a] pH = 7.4	pH = 8.0
Rb. sphaeroides	865	0.66	9.9	10.3
Rs. rubrum	865	0.61	9.3	9.3
Rs. centenum	850	0.85	7.6	7.9
Rb. capsulatus	850	0.84	7.5	7.8
Rb. capsulatus/DOC[c]	865	0.60	9.0	9.4

[a] From Wang et al. (1994). [b] Fraction of spin density on P_L (see Tables 1 and 2). Note that this value is essentially the same (0.66) in chromatophores for all four species. [c] Addition of 0.03% DOC for the optical absorption spectra and recombination kinetics and 0.1% for the EPR and ENDOR measurements.

Motivated by these findings, P^+ • in RCs of *Rb. capsulatus* solubilized in 0.1% LDAO have been measured with and without addition of DOC (0.1%). The respective Special TRIPLE spectra are shown in Figure 5. The P^+ • spectrum obtained from RC solutions containing DOC (Figure 5a) exhibits additional lines compared with the spectrum of untreated RCs (Figure 5b). Subtraction of the two spectra reveals the existence of a distinct additional second species in the DOC-treated sample characterized by sharp resonance lines comparable in line width to those of the first species (Figure 5c). The P^+ • spectrum of this second species is similar to that of *Rs. rubrum* (Figure 2). The respective hfcs are presented in Table 2.

The observation that the immediate environment of the RCs influences the electronic structure of the dimer in *Rb. capsulatus* and *Rs. centenum* led us to investigate the species P^+ • in its natural membrane environment, i.e., in chromatophores. The obtained EPR line widths of P^+ • in illuminated, frozen chromatophores were the same in all four investigated species (0.98 ± 0.02 mT) in contrast to the line widths observed in isolated RCs (see Table 1). A similar line width has been reported for P^+ • in *Rb. capsulatus* chromatophores (Bylina et al., 1990). Figure 6 shows the frozen solution ENDOR spectra of P^+ • in chromatophores of the four bacterial species.

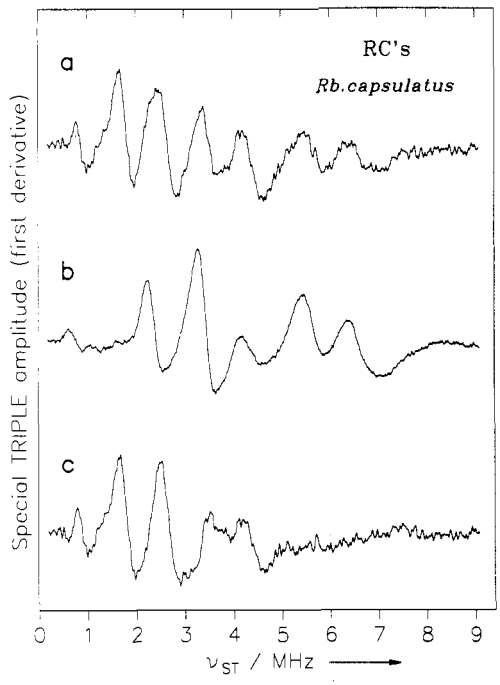

FIGURE 5: Comparison of the Special TRIPLE spectra of $P^+ \cdot$ in RCs of different samples of *Rb. capsulatus*. (a) RCs containing 0.1% LDAO and 0.1% DOC; (b) RCs with 0.1% LDAO; (c) difference spectrum (a) – (b). Experimental conditions: $T = 288$ K, microwave power 16 mW, rf power 2 × 150 W, rf modulation depth 200 kHz (frequency 12.5 kHz); accumulation time 4 h (a) and 2 h (b). For subtraction the spectra were normalized with respect to the largest two β-proton hfcs, which belong only to one, the more asymmetric, species.

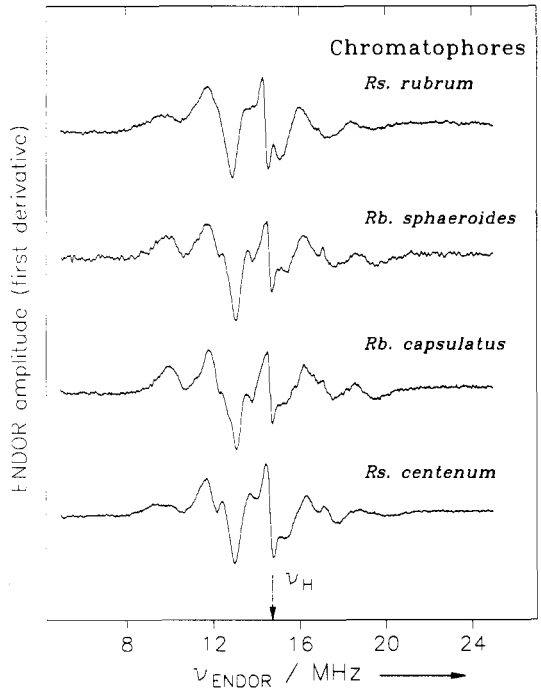

FIGURE 6: Comparison of the ENDOR spectra of light-induced $P^+ \cdot$ in chromatophores of *Rs. rubrum*, *Rb. sphaeroides*, *Rb. capsulatus*, and *Rs. centenum*. Experimental conditions for *Rs. rubrum* are T = 160 K, microwave power 4 mW, rf power 200 W, rf modulation depth 200 kHz (frequency 12.5 kHz), accumulation time 1 h. For the other species the conditions are $T = 150$ K, microwave power 4 mW, rf power 150 W, rf modulation depth 200 kHz (frequency 12.5 kHz), accumulation time 1 h.

The same *powder* ENDOR spectra were also obtained in *liquid* chromatophore solution at room temperature due to the slow tumbling motion of the large particles.

From Figure 6 it is obvious that the spectra of all four species are essentially identical apart from small variations in line widths and resolution. A complete analysis of the hfc tensors is difficult due to the strong overlap of spectral features. However, the hyperfine splittings read directly from the spectra are essentially the same for all four species. For *Rb. sphaeroides* the hfc tensors are known from measurements in RC single crystals (Lendzian et al., 1993). From these data, the respective $P^+ \cdot$ powder spectrum shown in Figure 6 can be simulated (data not shown), indicating that both the isotropic and anisotropic hfcs of $P^+ \cdot$ are essentially the same in RC single crystals and chromatophores. Comparison of the spectra in Figure 6 shows that the spin density distributions of $P^+ \cdot$ in chromatophores are very similiar in the four species and the ratio of the spin density on P_L versus P_M appears to be close to the value of 2:1 found for *Rb. sphaeroides*.

DISCUSSION

For $P^+ \cdot$ in RCs in their natural lipid environment, i.e., in chromatophores, the obtained spin density distribution is essentially the same in all investigated species. It is characterized by a spin density of approximately 65% residing on the L half and 35% on the M half of the dimer. This highly conserved asymmetry of $P^+ \cdot$ in all species—which has also been found in the BChl *b*-containing purple bacterium *Rps. viridis* (Lendzian et al., 1988)—could therefore be of key importance for the optimal function of the bacterial RC, e.g., for the stabilization of the charge-separated state and the rereduction of $P^+ \cdot$ by cytochrome.

The electronic distribution of $P^+ \cdot$ is not changed in isolated RCs of *Rb. sphaeroides* and *Rs. rubrum*. However, for $P^+ \cdot$ in RCs of *Rb. capsulatus* and *Rs. centenum*, the state found in chromatophores is not conserved but a second distinct state of $P^+ \cdot$ is detected with a significantly stronger localization of the unpaired electron on P_L (~85%). Obviously, the electronic and/or spatial structure of the RCs is influenced by the specific RC environment. That such effects play an important role for the electronic structure of $P^+ \cdot$ is demonstrated for RCs of *Rb. capsulatus* by the addition of charged detergents which causes $P^+ \cdot$ to switch back to the more delocalized state observed in chromatophores (see Figures 5 and 6).

In view of the results obtained for chromatophores, the different degrees of delocalization of the unpaired electron in $P^+ \cdot$ of isolated RCs are surprising. In this respect it is important to reconcile which factors influence the delocalization of the unpaired electron in $P^+ \cdot$. The asymmetry of the spin density distribution in $P^+ \cdot$ in *Rb. sphaeroides* has been interpreted in terms of a dimer model that assumes energetically different halves [for details see Plato et al. (1992)]. The parameters that influence the asymmetry of the spin density distribution are (i) the difference of the Coulomb energies, $\Delta\alpha$, between the two dimer halves P_L and P_M and (ii) the resonance integral, β_D, which is a measure of the strength of the interaction between P_L and P_M. Figure 7b shows the spin density ratio ρ_L/ρ_M as a function of $\Delta\alpha/\beta_D$. When this model is adapted for $P^+ \cdot$ in *Rb. sphaeroides*, the ratio $\Delta\alpha/\beta_D = 0.35$ is obtained from the experimental value ρ_L/ρ_M = 2:1 and a value of $\Delta\alpha = 0.11$ eV is obtained using $\beta_D = 0.30$ eV from an independent MO calculation on $P^+ \cdot$ based on the X-ray structure of Allen et al. (1987) [see Plato et al. (1992) and Rautter et al. (1992)]. Possible reasons for the different energies of the BChl *a* moieties are (i) different positions of the acetyl groups, (ii) differences in the puckering of the macrocycles, or (iii) asymmetric interactions with the protein environment.

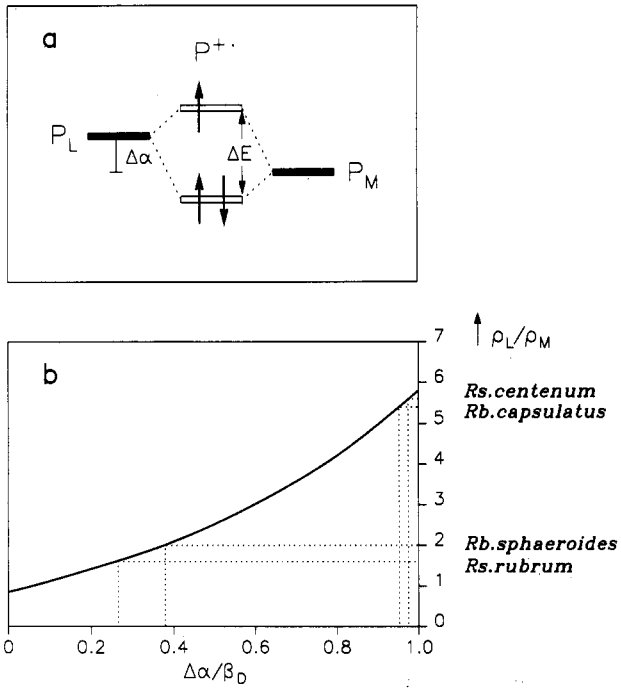

FIGURE 7: (a) Energy level scheme of the highest occupied molecular orbitals (HOMOs) of the monomeric halves P_L and P_M and of the two supermolecular orbitals of the dimer. $\Delta\alpha$ is the energetic difference (Coulomb integrals) of the L- and M-halves of the dimer: $\Delta\alpha = \epsilon_L - \epsilon_M$. The energy difference, ΔE, of the dimer orbitals contains $\Delta\alpha$ and β_D, the resonance integral between P_L and P_M (see text). For more details concerning this model, see Plato et al. (1992). (b) Relation between the ratio of the sums of spin densities ρ_L/ρ_M and the ratio of the energetic parameters $\Delta\alpha/\beta_D$ of a model dimer (two ethylene molecules) obtained from a HMO calculation (Plato et al., 1992). The ratios for $P^+\bullet$ in the RCs of the four investigated species are indicated by dotted lines (see text).

The energy difference ΔE between the resulting MOs of $P^+\bullet$ is given in this model by $\Delta E = [(\Delta\alpha)^2 + (2\beta_D)^2]^{1/2}$. The energy of this transition of the primary donor cation radical was recently measured by Breton et al. (1992), who found a new absorption band in the far-infrared region centered around 2600 cm^{-1} for *Rs. rubrum*, *Rb. sphaeroides*, and *Rb. capsulatus* chromatophores. In that paper, the transition was interpreted for the first time in terms of a dimer with energetically different halves. A more detailed and elaborate analysis of this model with the emphasis on optical transitions was provided by Parson et al. (1992). Based upon the calculated and observed dipole strengths of the band at 2600 cm^{-1}, the model predicts an asymmetric charge distribution in $P^+\bullet$. In a similiar model developed by Plato et al. (1992) for the calculation of the spin density distribution of $P^+\bullet$, the ratio of $\Delta\alpha/\beta_D$ can be obtained directly from the spin density ratio ρ_L/ρ_M (Figure 7b). Together with the experimental value of 2600 cm^{-1} for ΔE, which corresponds to 320 meV, this provides the possibility to experimentally assess the value for the resonance integral and energy difference between the two dimer halves, P_L and P_M. This approach yields $\beta_D = 0.16$ eV and $\Delta\alpha = 55$ meV for $P^+\bullet$ in *Rb. sphaeroides*. The model is used to further estimate the energetic shifts of $P^+\bullet$ in the other RCs studied here.

From the ratios of the hfcs at positions 1a and 5a given in Table 1, it can be deduced that the internal geometry of the two bacteriochlorophylls of the dimer is quite similar in all four RCs. The predominant experimental effect is a shift of spin density between the dimer halves. The observed spin density ratios ρ_L/ρ_M and corresponding values of $\Delta\alpha/\beta_D$ for the four different bacterial species are depicted in Figure 7b. If one assumes that the interaction energy, β_D, is the same in all four species (0.16 eV), an energy difference of $\Delta\alpha = 38$ meV is obtained for $P^+\bullet$ in *Rs. rubrum*. This differs only by −17 meV from the corresponding value for $P^+\bullet$ in *Rb. sphaeroides*. A more drastic effect occurs for $P^+\bullet$ in *Rb. capsulatus* and *Rs. centenum*, where the unpaired electron is almost completely localized on P_L (84% and 85%, respectively). Values of $\Delta\alpha = 135$ meV and $\Delta\alpha = 137$ meV are obtained for these two species (Figure 7), which correspond to an increase of the energetic difference between P_L and P_M by approximately +80 meV as compared with *Rb. sphaeroides*. Effects of this magnitude were observed in mutants of *Rb. sphaeroides* where an additional interaction with an amino acid residue that forms a hydrogen bond to the keto group in position 9 (Figure 1) of P_L or P_M was introduced (Williams et al., 1992; Rautter et al., 1992). However, the deduced changes of $\Delta\alpha$ for $P^+\bullet$ in RCs of the different species is difficult to explain by changes in the direct interactions (e.g., H-bonds) with key amino acid residues alone, since they are conserved in all four species (Komiya et al., 1988; Williams et al., unpublished results). Alternatively, the resonance integral β_D could be different for $P^+\bullet$ in RCs of the four species, caused by a difference in orbital overlap between the dimer halves.

It has been found that two *distinct* states of $P^+\bullet$ exist in the different RCs. Possible reasons for the different spin density ratios may be obtained from MO calculations which show that the rotation angle of the acetyl group at ring I has a major effect on the energy difference between P_L and P_M and constitutes the main contribution to $\Delta\alpha$ in *Rb. sphaeroides* (Plato et al., 1986, 1992). Different acetyl group orientations in the four species may be caused by different interactions with the surrounding protein that are not completely identical in isolated RCs. Near-infrared resonance Raman Fourier transform investigations (Mattioli et al., 1992) showed that the asymmetric hydrogen bonding situation between His L168 and the acetyl group at position C_2 (cf. Figure 1) on the L-half is conserved in *Rb. sphaeroides*, *Rb. capsulatus*, and *Rs. rubrum*. The vibrational frequency of this hydrogen-bonded acetyl group shows, however, slight but significant variations between the investigated species that indicates different hydrogen-bonding interactions between the histidine and the acetyl group. These differences could be responsible for the different Coulomb energies of the dimer halves.

The electron transfer rates involving $P^+\bullet$ are determined by a number of parameters, such as the energy difference between the initial and final states, reorganization energy, etc. [for a review see Marcus and Sutin (1985)]. For RCs from the different purple bacteria, many of the electron transfer rates are very similar (Wang et al., 1994). Assuming that all other parameters are the same, then it is possible to compare the measured rates of these species for charge recombination from the primary quinone with the observed orbital asymmetries of $P^+\bullet$ in these RCs (Table 3). The observed asymmetry in $P^+\bullet$ is associated with the highest occupied molecular orbital (HOMO) of the dimer. The HOMO is expected to play an important role in the stabilization of the charge-separated state by influencing the back electron transfer rate. In an asymmetric dimer, where the hole is predominantly located on the dimer half remote from the active branch, a slower recombination rate is expected. Inspection of the recombination rates from the primary quinone at different pH values (Table 3) indicates somewhat slower recombination rates for *Rb. capsulatus* and *Rs. centenum* (Wang et al., 1994), which also show a larger orbital asymmetry for $P^+\bullet$ than *Rb.*

sphaeroides and *Rs. rubrum*. In the presence of DOC, the spin density of $P^{+}\bullet$ in *Rb. capsulatus* becomes more symmetrical and the recombination rate increases to a value comparable to that of *Rb. sphaeroides* (Wang et al., 1994). The pH dependence of the recombination rates (Table 3) is probably due to interactions involving the ubiquinone radical anion, $Q_A^{-}\bullet$, and protonatable residues as discussed elsewhere (Wang et al., 1994). This is supported by the fact that the spin density distribution of $P^{+}\bullet$ in *Rb. sphaeroides* is not changed between pH 7.5 and 10.

It has been observed that there are only two different spin density distributions in the RCs of the four species: in *Rb. sphaeroides* and *Rs. rubrum* ~65% of the unpaired electron is on P_L and ~35% is on P_M, whereas in *Rb. capsulatus* and *Rs. centenum* ~85% is on P_L and ~15% is on P_M. This corresponds to two distinct conformations of the dimer in these species. Under certain conditions both conformations are present in the same RC sample. This is demonstrated for the case of *Rb. capsulatus* by the addition of the charged detergent DOC (Figure 5). In all investigated RCs, similar effects could be produced by freezing and thawing the samples (Rautter et al., unpublished data). Obviously, these two states exist in all four investigated species. In chromatophores only one of these states is detected, i.e., the more symmetric one. Whether the asymmetric state also exists in chromatophores is not clear at present.

It may be speculated that, concurrent with either electron transfer or excitation of the dimer, conformational changes involving these two states may occur that facilitate the fast unidirectional electron transfer and stabilize the charge-separated states. A similar "conformational switching" has been proposed earlier for electron transfer involving the pheophytin in plant photosystem II (Lubitz et al., 1989). In the same way the acetyl groups of P_L and P_M could act as conformational switches in the primary donor of purple bacteria. Currently, ENDOR experiments on mutants in the vicinity of the C_2 acetyl groups of the dimer in *Rb. sphaeroides* are in progress to further investigate the role of the orientation of these groups for the spin density distribution of $P^{+}\bullet$.

ACKNOWLEDGMENT

We thank Irene Geisenheimer (Technische Universität) for the preparation of the reaction centers of *Rs. rubrum* G-9 and Dr. Robert Bittl and Wolfgang Zweygart (Technische Universität) for writing the program used for the control of the ENDOR/TRIPLE section of the spectrometer. Many helpful discussions concerning the dimer model with Dr. Martin Plato (Freie Universität Berlin) are gratefully acknowledged.

REFERENCES

Allen, J. P., Feher, G., Yeates, T. O., Komiya, H., & Rees, D. C. (1987) *Proc. Natl. Acad. Sci. U.S.A. 84*, 5730–5734.

Allendoerfer, R. D., & Maki, A. H. (1970) *J. Magn. Reson. 3*, 396–410.

Breton, J., Nabedryk, E., & Parson, W. W. (1992) *Biochemistry 31*, 7503–7510.

Bylina, E. J., Kolaczkowski, S. V., Norris, J. R., & Youvan, D. C. (1990) *Biochemistry 29*, 6203–6210.

Deisenhofer, J., Epp, O., Miki, K., Huber, R., & Michel, H. (1984) *J. Mol. Biol. 180*, 385–398.

El-Kabbani, O., Chang, C. H., Tiede, D., Norris, J., & Schiffer, M. (1991) *Biochemistry 30*, 5361–5369.

Feher, G. (1992) *J. Chem. Soc., Perkin Trans. 2 11*, 1861–1874.

Feher, G., Hoff, A. J., Isaacson, R. A., & Ackerson, L. A. (1975) *Ann. N.Y. Acad. Sci. 244*, 239–259.

Forman, A., Renner, M. W., Fujita, E., Barkigia, K. M., Evans, M. C., Smith, K. M., & Fajer, J. (1989) *Isr. J. Chem. 29*, 57–64.

Gessner, Ch., Lendzian, F., Bönigk, B., Plato, M., Möbius, K., & Lubitz, W. (1992) *Appl. Magn. Reson. 3*, 763–777.

Huber, M., Lous, E. J., Isaacson, R. A., Feher, G., Gaul, D., & Schenck, C. C. (1990) in *Reaction Centers of Photosynthetic Bacteria* (Michel-Beyerle, Ed.) pp 219–228, Springer Verlag, Berlin.

Hyde, J. S., Rist, G. H., & Eriksson, L. E. G. (1968) *J. Phys. Chem. 72*, 4269.

Käss, H., Rautter, J., Zweygart, W., Struck, A., Scheer, H., & Lubitz, W. (1994) *J. Phys. Chem. 98*, 354–363.

Komiya, H., Yeates, T. O., Rees, D. C., Allen, J. P., & Feher, G. (1988) *Proc. Natl. Acad. Sci. U.S.A. 85*, 9012–9016.

Lendzian, F., Lubitz, W., Scheer, H., Hoff, A. J., Plato, M., Tränkle, E., & Möbius, K. (1988) *Chem. Phys. Lett. 148*, 377–385.

Lendzian, F., Huber, M., Isaacson, R. A., Endeward, B., Plato, M., Bönigk, B., Möbius, K., Lubitz, W., & Feher, G. (1993) *Biochim. Biophys. Acta 1183*, 139–160.

Lubitz, W. (1991) in *Chlorophylls* (Scheer, H., Ed.) pp 903–944, CRC Press, Boca Raton, FL.

Lubitz, W., Lendzian, F., Scheer, H., Gottstein, J., Plato, M., & Möbius, K. (1984) *Proc. Natl. Acad. Sci. U.S.A. 81*, 1401–1404.

Lubitz, W., Isaacson, R. A., Okamura, M. Y., Abresch, E. C., Plato, M., & Feher, G. (1989) *Biochim. Biophys. Acta 977*, 227–232.

Marcus, R. A., & Sutin, N. (1985) *Biochim. Biophys. Acta 811*, 265–322.

Mattioli, T. A., Robert, B., & Lutz, M. (1992) in *The Photosynthetic Bacterial Reaction Center II: Structure, Spectroscopy and Dynamics* (Breton, J., & Vermeglio, A., Eds.) pp 127–132, Plenum Press, New York.

McDowell, L. M., Gaul, D., Kirmaier, C., Holten, D., & Schenck, C. C. (1991) *Biochemistry 30*, 8315–8322.

Möbius, K., Lubitz, W., & Plato, M. (1989) in *Advanced EPR* (Hoff, A. J., Ed.) pp 441–499, Elsevier, Amsterdam.

Norris, J. R., Uphaus, R. A., Crespi, H. L., & Katz, J. J. (1971) *Proc. Natl. Acad. Sci. U.S.A. 68*, 625–628.

Parson, W. W., Nabedryk, E., & Breton, J. (1992) in *The Photosynthetic Bacterial Reaction Center II: Structure, Spectroscopy, and Dynamics* (Breton, J., & Vermeglio, A., Eds.) pp 79–88, Plenum Press, New York.

Plato, M., Tränkle, E., Lubitz, W., Lendzian, F., & Möbius, K. (1986) *Chem. Phys. 107*, 185–196.

Plato, M., Lendzian, F., Lubitz, W., & Möbius, K. (1992) in *The Photosynthetic Bacterial Reaction Center II: Structure, Spectroscopy and Dynamics* (Breton, J., & Vermeglio, A., Eds.) pp 109–118, Plenum Press, New York.

Rautter, J., Gessner, Ch., Lendzian, F., Lubitz, W., Williams, J. C., Murchison, H. A., Wang, S., Woodbury, N. W., & Allen, J. P. (1992) in *The Photosynthetic Bacterial Reaction Center II: Structure, Spectroscopy and Dynamics* (Breton, J., & Vermeglio, A., Eds.) pp 99–108, Plenum Press, New York.

Thanner, R. (1990) Diploma Thesis, Universität Stuttgart, Germany.

Tränkle, E., & Lendzian, F. (1989) *J. Magn. Reson. 84*, 537–547.

Yeates, T. O., Komiya, H., Rees, D. C., Allen, J. P., & Feher, G. (1988) *Proc. Natl. Acad. Sci. U.S.A. 85*, 7993–7997.

Wang, S., Lin, X., Woodbury, N. W., & Allen, J. P. (1994) *Photosynth. Res.* (submitted for publication).

Williams, J. C., Alden, R. G., Murchison, H. A., Peloquin, J. M., Woodbury, N. W., & Allen, J. P. (1992) *Biochemistry 31*, 11029–11037.

Zweygart, W., Thanner, R., & Lubitz, W. (1994) *J. Magn. Reson., Ser. A 109*, 172–176.